NANO LETTERS

2009
Vol. 9, No. 8
3066-3071

FRET Enhancement in Multilayer Core−Shell Nanoparticles

Mathieu Lessard-Viger, Maxime Rioux, Luc Rainville, and Denis Boudreau*

Département de chimie et Centre d'optique, photonique et laser (COPL), Université Laval, Québec (QC), Canada, G1V 0A6

Received May 14, 2009; Revised Manuscript Received June 25, 2009

ABSTRACT

This study describes the preparation and characterization of novel multilayer core−shell nanoparticles displaying metal-enhanced Förster resonant energy transfer. The increase in range and efficiency of Förster resonant energy transfer in these fluorescent nanocomposites and their vastly improved luminosity make them promising optical probes for a variety of applications such as cell imaging and biosensing.

Förster resonance energy transfer (FRET), a mechanism describing the nonradiative and distance-dependent energy transfer between two chromophores, is a powerful tool used in several fields of science. In physical chemistry and in biophysics, it is widely used in the study of a variety of biological phenomena, such as protein−protein and protein−DNA interactions, protein conformational changes, and other molecular dynamics.[1−7] FRET can provide information on the spatial relationship between two fluorophore-labeled sites in biological structures and macromolecules,[8,9] and FRET imaging has become an increasingly popular microscopy technique for the characterization of molecular interactions in living organisms.[10,11] The intermolecular sensing capacity of FRET is also extensively used in bioanalytical and biosensing applications, and numerous examples abound of the use of a donor-labeled DNA probe and a DNA target labeled with the acceptor, resulting in the observation of a dramatic increase in FRET between the two fluorophores upon DNA hybridization.[12−14]

The requirements for efficient FRET include close proximity of the donor and acceptor molecules, high molar absorptivity (for the donor) and high quantum yield (for the acceptor), as well as satisfactory photostability. The natural decay rate of the donor should also be lower than the energy transfer rate of the FRET donor−acceptor pair, to increase the probability of energy transfer to the acceptor before the donor fluoresces.[15] However, when classical fluorophores or fluorescent analogs of biomolecules are used as FRET donors or acceptors, their limited photostability, combined with extended sample illumination times or the use of high excitation irradiance, very often result in photodegradation, which biases the relationship between the fluorescence intensity of both chromophores and decreases the measured FRET efficiency. Moreover, FRET is a very short-range effect (<100 Å) and only occurs within closely spaced donor−acceptor pairs. Consequently, FRET efficiency is dramatically reduced for intermolecular distances beyond the Förster range (R_0, 20−55 Å for most organic fluorophores[1,16]) thereby hindering its use in imaging and biosensing applications where a longer interaction range would be needed.

Interestingly, the efficiency and range of FRET can be significantly increased by placing the donor−acceptor pairs in proximity to metal nanoparticles and exploiting the phenomenon called metal-enhanced fluorescence (MEF),[17,18] which affects the emission of nearby fluorophores by enhancing excitation and emission rates and improves FRET efficiency by increasing the strength of donor−acceptor interactions. Because MEF is most efficient when the metal and fluorophore are separated by several nanometers in order to avoid quenching by the metal,[19] previous investigations of MEF-enhanced FRET were carried out on metal nanoparticle films deposited on pairs of parallel quartz plates between which a dye solution was flowed.[16,20,21] Other investigations involved spectroscopic probing of individual nanoparticles functionalized with organic spacer molecules and conjugated with fluorophore-tagged DNA oligonucleotides.[22,23]

The development of core−shell nanostructures that display MEF, that is, metallic nanoparticles (NP) coated with a shell of silica doped with a suitable fluorophore, was reported recently.[24−28] These core−shell MEF-capable nanoparticles provide several advantages. The interaction with the metal core, usually silver or gold, greatly improves excitation efficiency and enhances the emissive rates, and the ensuing reduction of self-quenching makes possible the incorporation of larger amounts of dye molecules into the silica shell, whereas the shell protects the organic dyes against collisional quenching and irreversible photodegradation and provides

* To whom correspondence should be addressed. Phone: (418) 656-3287. Fax: (418) 656-7916. E-mail: denis.boudreau@chm.ulaval.ca.

10.1021/nl901553u CCC: $40.75
Published on Web 07/15/2009

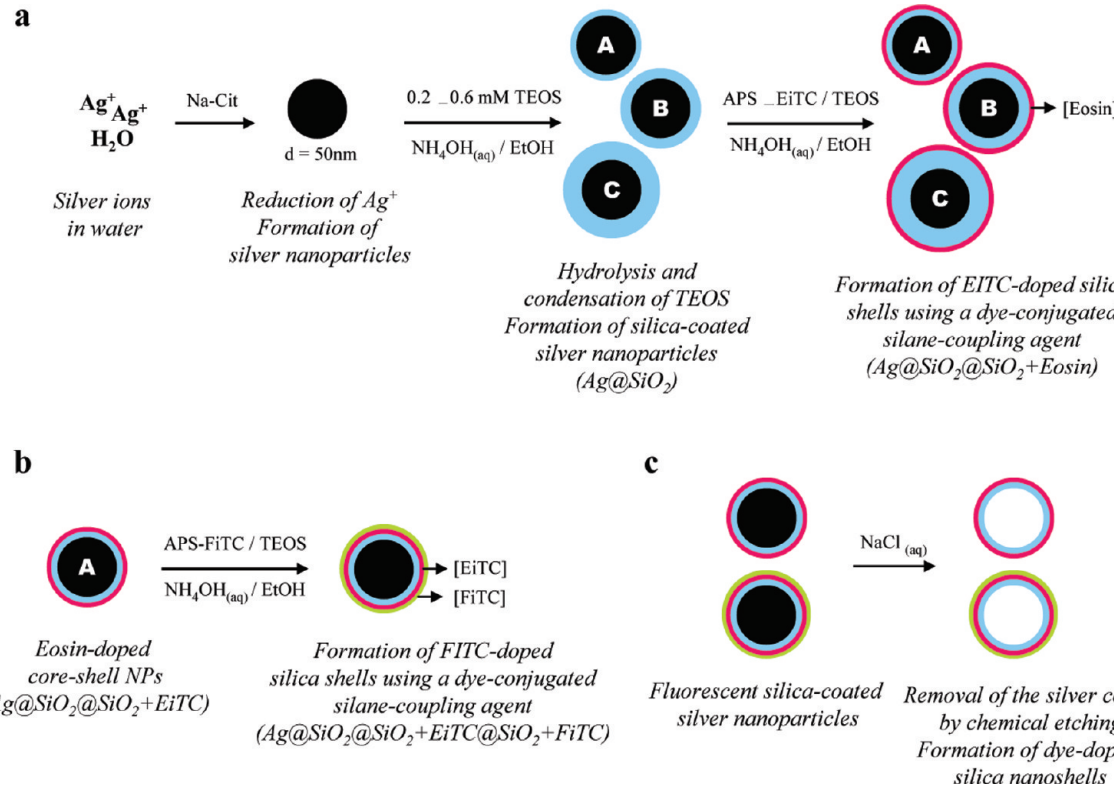

Figure 1. Schematic representation. (a) Preparation of eosin-doped silica-coated silver nanoparticles; (b) addition of fluorescein-doped silica shells onto eosin-doped silica-coated silver nanoparticles; (c) preparation of dye-doped hollow silica nanoshells by dissolution of the silver core.

easy conjugation to target biomolecules. Furthermore, the mobility of these nanoparticles is an asset for probing the contents of extended sample volumes in biosensing applications or for cell imaging work.

In the present work, we investigated the effect of MEF on FRET using Ag-core/SiO_2 spacer/SiO_2 + acceptor/SiO_2 + donor nanocomposites, where the spacer thickness is adjusted to optimize the metal-fluorophores distance and the fluorescence enhancement. Our concentric multilayer architecture (Figure 1) features a silver core on which is first grown a silica spacer shell with a controlled and uniform thickness to prevent quenching of the fluorescence by the metal at very close range. A fluorescent dye (the acceptor) is then covalently incorporated in a second silica shell (Figure 1a), followed by the deposition of a donor-labeled silica shell onto the acceptor-labeled silica-coated silver NP (Figure 1b). This controlled geometry allows us to study the effect of a metallic silver core at a fixed and controlled distance from the donor−acceptor pair. We chose fluorescein-5′-isothiocyanate (FiTC) as the energy donor and eosin-5′-isothiocyanate (EiTC) as the energy acceptor because of their well-documented photophysical characteristics and their overlapping absorption and emission bands.

Well-dispersed spherical Ag@SiO_2 core−shell nanocomposites were obtained using a standard citrate reduction along with an improved Stöber process. The prepared citrate-stabilized silver NPs have an average size of 47 ± 7 nm and present suitable plasmon absorption for MEF with the chosen dyes. It is known that the size of the metal core can have an influence on MEF, and it was recently reported that the enhancement efficiency of MEF for fluorophores near the surface of silver nanoparticles reaches a maximum for particle size around 50 nm and remains relatively constant in the 40−70 nm range,[29] therefore we can assume that MEF efficiency will be relatively uniform across the span of our core−shell nanoparticles (47 ± 7 nm). Uniform silica spacer shells were grown onto the silver NPs and the amount of TEOS used in the synthesis was adjusted to vary the thickness of the spacer shell from 7 to 23 nm in order to optimize the fluorescence enhancement (Figure 2). Interestingly, no silica particles without silver cores were found in the samples, and this method provides pure silica surfaces on silver NPs without the need for lengthier procedures such as surface activation or initial silica deposition with sodium silicate.[30,31]

The synthesis of Ag@SiO_2 NPs was followed by the growth of a second, thinner dye-doped silica shell (3 nm) in which EiTC was covalently incorporated. The use of a fluorescent dye silica precursor ensures the stability of the luminescence of NPs over time, and tests with year-old samples have confirmed that no significant dye leaching to solution occurred in that time period. Many fluorescent Ag@SiO_2@SiO_2 + EiTC samples with increasing EiTC concentration were prepared from each Ag@SiO_2 stock solution (7 ± 2, 13 ± 2, 23 ± 3 nm thick spacers) to determine the influence on fluorescence intensity and lifetime of metallic core proximity and of self-quenching between eosin molecules (Figure 3). The recorded fluorescence data shows that the relative emission yield reaches a maximum for core−shell NPs with a dye concentration of approxi-

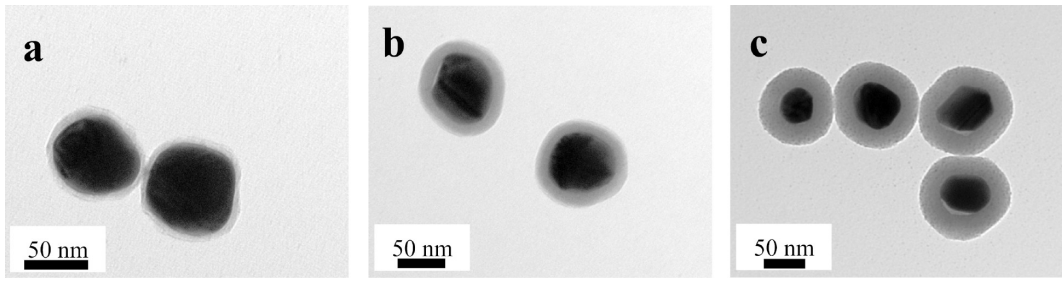

Figure 2. Transmission electron microphotographs of silica-coated silver nanoparticles with different thicknesses of the silica coating, controlled by the amount of TEOS incorporated to the reaction mixture. (a) [TEOS] = 0.2 mM, $t_{SiO2} = 7 \pm 2$ nm; (b) [TEOS] = 0.4 mM, $t_{SiO2} = 13 \pm 2$ nm; (c) [TEOS] = 0.6 mM, $t_{SiO2} = 23 \pm 3$ nm.

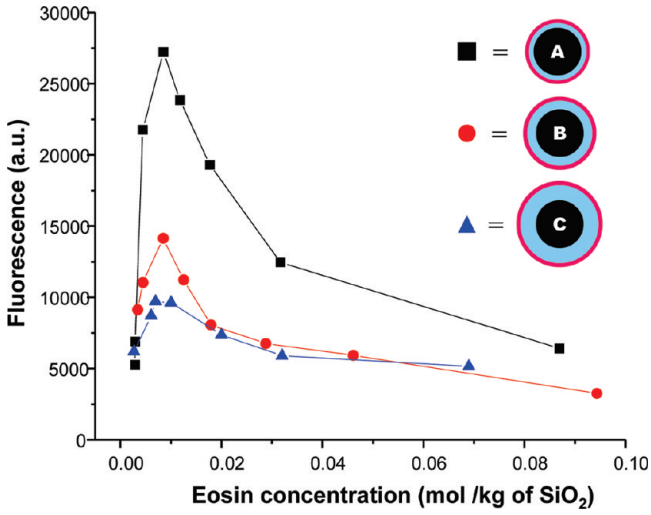

Figure 3. Influence of metal core proximity and of eosin concentration on the fluorescence intensity of $Ag@SiO_2@SiO_2$ + eosin composites nanoparticles. Three different spacer thicknesses were studied (A, 7 ± 2 nm; B, 13 ± 2 nm; C, 23 ± 3 nm). The excitation wavelength was 520 nm.

mately 10 mM (0.01 mol of eosin per kg of SiO_2). Beyond this dye concentration, a pronounced decrease in fluorescence intensity is observed, a typical manifestation of self-quenching corroborated by an expected red shift of the emission maximum of the dye.[25,32] The highest luminescence intensity was observed for the NPs with the thinnest spacer shell (7 ± 2 nm), which is in accordance with previous reports.[19,33] The distance dependence of MEF is shown in Figure 3, where the luminescence intensity is shown to drop rapidly when the spacer thickness is increased.

To confirm the influence of the metal cores on fluorescence emission, control samples (hollow silica nanoshells) were prepared from fluorescent core−shell NPs by dissolving the silver cores with chloride ions (Figure 4). This resulted in a pronounced drop of fluorescence intensity simultaneously with the disappearance of the plasmonic absorption band. No leaching of the fluorophores, which are covalently linked to the silica, was observed following this etching process.

The absorption spectra of $Ag@SiO_2@SiO_2$ + eosin nanocomposites and hollow silica nanoshells containing different amounts of EiTC are shown in Figure 5. The absorption spectrum for the core−shell nanoparticles is dominated by the absorption band centered around 420 nm that corresponds to the plasmonic absorption from the silver cores (Figure 5, upper curve). The complete dissolution of the metal cores by chloride ions is confirmed by the disappearance of the plasmonic band at 420 nm from the absorption spectra recorded for the nanoshell samples (Figure 5, lower curves). The intensity of the EiTC absorption band at 520 nm increases with concentration, an indication that controlled dye incorporation into the core−shell NPs using a silane coupling agent was effective and that the covalent binding resisted the etching of the silver core.

Comparison of the fluorescence spectra recorded from fluorescent core−shell nanocomposites at different dye-to-metal separations with that from their respective nanoshell control samples shows a significant increase of the fluorescence yield in the presence of the metal core, that is, a 15-fold increase for a dye-to-metal separation of 7 ± 2 nm, and lesser enhancement ratios of 5 and 2 for spacer thicknesses of 13 ± 2 and 23 ± 3 nm, respectively (Supporting Information, Figure S1). Since smaller silica spacer shells (<5 nm) could not be deposited on the silver colloids with sufficient uniformity using the current procedure, it is not known whether the luminescence from metal cores protected by an even thinner spacer would display a greater enhancement or would be dominated by quenching by the metal. Interestingly, Wokaun et al. reported a maximum luminescence enhancement of 200 for a 25 Å thick evaporated layer of SiO_2 on a planar silver island film.[19]

Since the enhancement of fluorescence close to a metallic surface is known to be accompanied by a decrease in the lifetime of excited states, fluorescence lifetime measurements are a useful indicator of MEF. Fluorescence decay curves were acquired for both core−shell NPs and their corresponding hollow silica nanoshells, and the results show that the core−shell NPs systematically have a faster decay than their corresponding hollow nanoshells and the free fluorophore molecules, for example, a fluorescence lifetime of 0.228 ns was determined for eosin in the NPs with a 7 ± 2 nm thick spacer, which corresponds to a 8- and 13-fold reduction in lifetime as compared to eosin molecules bound to bare silica and free in solution, respectively (Supporting Information, Table S1). This observation is a manifestation of the MEF phenomenon, in which metal-fluorophore interactions lead to an increase in the quantum yield of the fluorophore and a decrease in its lifetime.[34−36] Furthermore, the largest fluorescence enhancement is associated with the most dramatic decrease in excited state lifetime and the shortest metal-

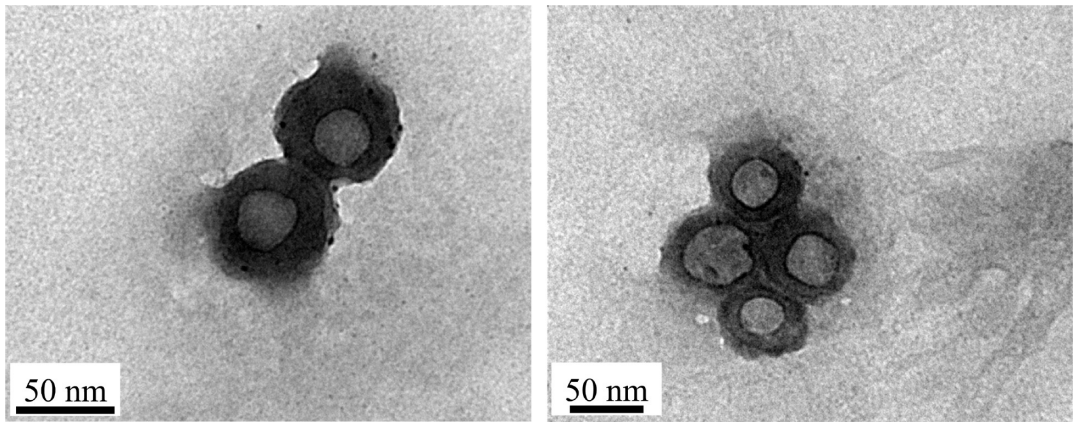

Figure 4. Transmission electron micrographs of hollow silica nanoshells prepared from core−shell nanoparticles.

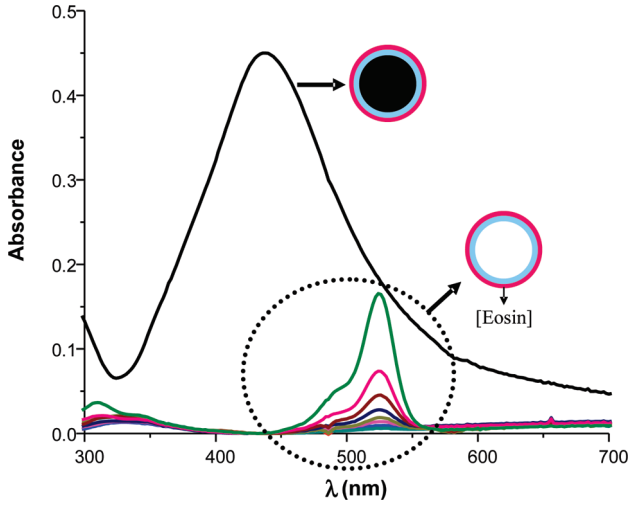

Figure 5. Absorption spectra of $Ag@SiO_2@SiO_2$ + eosin nanocomposites (upper curve) and hollow silica nanoshells (lower curves). The thickness of the silica spacer shell was 7 ± 2 nm and the concentration of EiTC was 4 mM in the core−shell nanoparticles (upper curve) and was varied from 0 to 87 mM in the dye-doped hollow silica shells (lower curves).

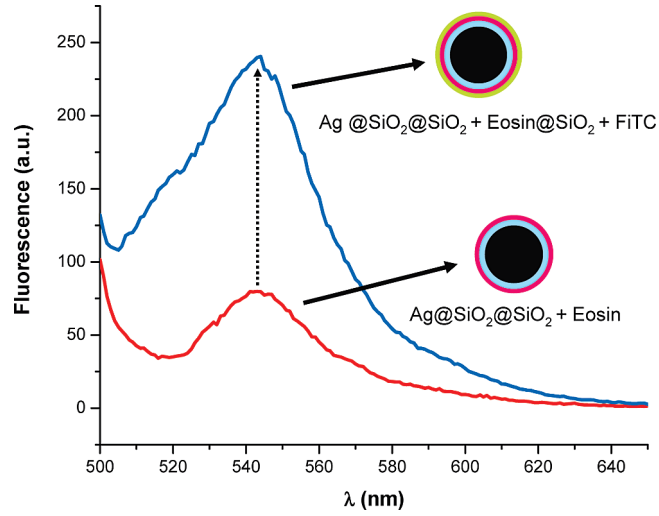

Figure 6. Comparison of the fluorescence spectra recorded for donor/acceptor multishell and acceptor-only core−shell nanocomposites; [FiTC] = 7.2 mM, [EiTC] = 8.5 mM). The excitation wavelength was 485 nm.

fluorophore distance (7 ± 2 nm), whereas the thicker silica spacers result in lower fluorescence intensity and longer lifetime. Interestingly, since the photostability of fluorophores depends, among other factors, on their recycling time (i.e., lifetime of their excited states), these $Ag@SiO_2@SiO_2$ + eosin core−shell nanocomposites should display enhanced robustness toward photodestructive processes and thereby giving a substantial increase in number of detectable photons.

To establish a FRET system in these core−shell nanoparticles, a donor-labeled silica shell was conjugated onto the acceptor-labeled silica-coated silver NPs with the thinnest spacer. Using the same synthetic procedure previously used to graft EiTC within the first dye-doped silica shell, we were able to deposit another very thin (∼3 nm) silica layer containing varying amounts of FiTC on the $Ag@SiO_2@SiO_2$ + EiTC nanocomposites. Keeping both fluorescent shells at a minimal thickness and in direct contact maximizes the number of donors and acceptors within the Förster range achievable with these core−shell nanostructures. We chose to position the acceptor (eosin) closer to the metal core because it has a lower quantum yield than fluorescein.[1] Since MEF is caused by the near-field interaction of a fluorophore with a metal particle, and FRET occurs by dipole−dipole interaction between an excited donor and an acceptor, it is reasonable to assume that metal-enhanced FRET is due to near-field interaction between the donor−acceptor pair and the electric field near the metal particle, and that the efficiency of FRET enhancement will be correlated with the dependence of MEF on distance to the metal core.[37] The data of Figure 3 suggests that the efficiency of MEF for eosin can drop significantly across a distance as small as the thickness of the eosin-labeled layer (i.e., ∼3 nm). Therefore, FRET efficiency benefits the most by placing eosin closest to the metal core.

Figure 6 shows fluorescence spectra recorded for donor/acceptor multishell nanocomposites and their corresponding acceptor-only core−shell NPs (i.e., before coating with the donor). Comparison of the spectra shows an ∼3 times increase in the emission of the acceptor at 545 nm upon the addition of the donor, despite the fact that the acceptor concentration is the same in both types of nanocomposites. Only a slight contribution of donor emission at 520 nm is perceivable in the spectrum of the multishell sample. These results clearly indicate the presence of resonant energy

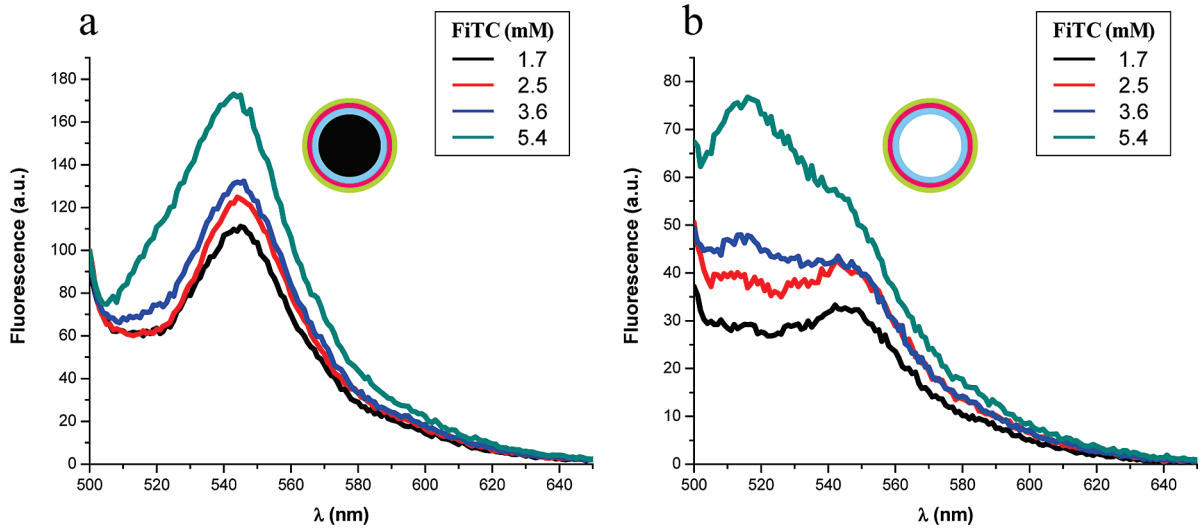

Figure 7. Fluorescence spectra recorded for donor/acceptor multishell nanoparticles (a) and corresponding hollow silica nanoshells (b) in which the concentration of FiTC (donor) was increased from 1.7 to 5.4 mM, while the concentration of EiTC (acceptor) was kept constant at 12 mM. The excitation wavelength was 485 nm.

transfer from the donor to the acceptor. The high acceptor/donor emission ratio observed with these nanocomposites results from a very efficient resonant energy transfer process combined with the higher nominal absorptivity of the donor at the excitation wavelength used for this experiment (ε_{485}^{FITC} = 90227 L·mol^{-1}·cm^{-1}, ε_{485}^{EITC} = 26688 L·mol^{-1}·cm^{-1}).[38]

The influence of plasmonic coupling to the metal core on the extent of FRET between donor and acceptor was studied by comparing the fluorescence spectra recorded before and after dissolution of the metal core, for a fixed concentration of EiTC and various FiTC concentrations (Figure 7). It was found that, in the presence of the silver core, the emission intensity of the eosin acceptor at 545 nm increases as the fluorescein donor concentration in the nanoparticles is increased, and that donor emission at 520 nm is barely perceptible (Figure 7a). On the other hand, increasing the amount of donor molecules on the surface of coreless nanoparticles results mainly in the increase of donor emission intensity (Figure 7b), an indication that FRET efficiency between FiTC and EiTC is relatively poor in the coreless multishell NPs, despite the relative proximity of the FiTC and EiTC layers. The results shown in Figure 7 are in agreement with an enhancement of FRET efficiency for donor and acceptor fluorophores located near silver particles.

It is well known that any increase in resonant energy transfer between a donor and an acceptor will be accompanied by a decrease in the fluorescence decay time of the donor. Fluorescence decay curves of fluorescein were recorded for core−shell nanoparticles and corresponding hollow silica nanoshells for a fixed concentration of eosin (acceptor) molecules and variable fluorescein (donor) concentrations (Supporting Information, Table S2). The results show that in the presence of the silver cores fluorescein lifetime decreases from 0.077 to 0.056 ns as fluorescein concentration is increased. It is unlikely that these shorter lifetimes are caused by increasing self-quenching between fluorescein molecules, since we measured constant lifetimes for the corresponding hollow silica nanoshells. A more plausible explanation is that the increasing concentration of fluorescein in the outer silica shell, assuming that fluorophore molecules are randomly distributed in the silica, reduces the average donor−acceptor distance and gradually brings the donor and acceptor molecules within the Förster range, which in turn enhances resonant energy transfer and leads to the observed decrease in donor lifetime. Interestingly, the average intermolecular distance between FiTC molecules in the silica matrix, calculated from the concentration data, varies from ∼79 to ∼55 Å, thus becoming progressively closer to the Förster distance published for the FiTC-EiTC system, that is, ∼54 Å.[39] In the case of the hollow nanoshell samples, intermolecular distances are still too large to induce significant RET without the assistance of MEF, which is consistent with the constant lifetimes and the absence of significant FRET in coreless samples (Figure 7b).

FRET efficiency (E) can be determined by comparing the lifetime of the donor alone (τ_{DA}) and in the presence of the acceptor (τ_D) using the relationship $E = 1 - [(\tau_{DA})/(\tau_D)]$.[1] Using the results of the lifetime analysis (Supporting Information, Table S3), transfer efficiencies of 12 and 56% are calculated for the hollow silica nanoshells and the core−shell nanoparticles, respectively. These transfer efficiency values can then be used to calculate the average donor−acceptor distance (R) or the Förster distance (R_0), that is, the distance between donor and acceptor molecules at which the energy transfer efficiency is 50%, using the relationship $E = R_0^6/[R_0^6 + R^6]$.[1] Using a R_0 of 54 Å for the fluorescein−eosin system and a transfer efficiency of 12% for the hollow silica nanoshells, an average distance between fluorescein and eosin of 75 Å is calculated. Since silica shells are rigid and the fluorophores are covalently attached to them, the average donor−acceptor distance is expected to be the same in Ag@SiO$_2$@SiO$_2$ + eosin@SiO$_2$ + fluorescein NPs and in their corresponding hollow silica nanoshells. Consequently, using an R equal to 75 Å and a transfer efficiency of 56%, an apparent Förster distance R_0 of 78 Å is calculated, or an increase of ∼30% for these multilayer core−shell

nanocomposites. This increase in Förster distance suggests the use of such multilayer core−shell fluorescent NPs for imaging microscopy and biosensing applications, in which they could be conjugated to biomolecules and used as longer range donor−acceptor pairs. It is interesting to note that the fluorescence lifetime measured for fluorescein in the presence of the silver core (i.e., in core−shell nanoparticles featuring the 7 nm spacer) is ∼80 times shorter than that of fluorescein in hollow silica nanoshells and ∼110 times shorter than that of fluorescein molecules freely diffusing in solution. This dramatic reduction of the time spent by fluorescein in the excited state is attributable to the conjunction of FRET and MEF in multilayer core−shell NPs and should translate to an enhanced photostability and increased detectability for such nanocomposites when excited at high excitation irradiances.

In this work, we were able to fabricate, using a versatile, simple and reproducible procedure, a multilayer nanoarchitecture featuring a metal core surrounded by concentric silica layers containing FRET donor and acceptor molecules positioned at precise distances from the core. Our study shows that the presence of the metal core results in an increase in Förster efficiency by a factor of 4 and an increase in Förster range of ∼30%. Our study also shows that the luminosity of the fluorophores is increased several-fold by the metal-enhanced fluorescence displayed in these core−shell nanocomposites, and that the lifetime of their excited states is reduced by as much as 2 orders of magnitude, resulting in enhanced photostability and detectability of these nanoparticles. The fluorophores grafted within these core−shell nanoparticles are very stable, with no indication of leaching to the surrounding solution after extended periods of time. Moreover, by varying the dyes and their relative concentrations and by tuning their emission signatures, such nanocomposites could also be adapted to multiplexed signaling. Given these enviable characteristics, these multilayer core−shell fluorescent NPs could therefore provide increased detectability, range and efficiency of Förster resonant energy transfer in a variety of applications such as ultrasensitive DNA detection, long exposure FRET imaging studies, and the study of long-range extracellular protein−protein, cell−protein and cell−cell interactions.

Acknowledgment. We are grateful to the Natural Sciences and Engineering Research Council of Canada, the "Fonds Québécois de la Recherche sur la Nature et les Technologies du Québec", the Canadian Foundation for Innovation and the Canadian Blood Services for financial support of this research. The authors would like to express their gratitude to PicoQuant for their assistance in lifetime measurements, to Maurice Boissinot and Karel Boissinot for the cover artwork, and to Dr. Kim Doré for inspiring exchanges.

Supporting Information Available: Details of experimental methods and tabulated fluorescence lifetime analysis data. This material is available free of charge via the Internet at http://pubs.acs.org.

References

(1) Lakowicz, J. R. *Principles of Fluorescence Spectroscopy*, 2nd ed.; Plenum Publishing Corporation: New York, 1999.
(2) Truong, K.; Ikura, M. *Curr. Opin. Struct. Biol.* **2001**, *11*, 573.
(3) Day, R. N.; Periasamy, A.; Schaufele, F. *Methods* **2001**, *25*, 4.
(4) Cremazy, F. G. E.; Manders, E. M. M.; Bastiaens, P. I. H.; Kramer, G.; Hager, G. L.; van Munster, E. B.; Verschure, P. J.; Gadella, T. J.; van Driel, R. *Exp. Cell Res.* **2005**, *309*, 390.
(5) Giannetti, A.; Citti, L.; Domenici, C.; Tedeschi, L.; Baldini, F.; Wabuyele, M. B.; Vo-Dinh, T. *Sens. Actuators, B* **2006**, *B113*, 649.
(6) Kajihara, D.; Abe, R.; Iijima, I.; Komiyama, C.; Sisido, M.; Hohsaka, T. *Nat. Methods* **2006**, *3*, 923.
(7) Lorenz, M.; Diekmann, S. *Methods Mol. Biol.* **2006**, *335*, 243.
(8) Kasprzak, A. A. *Methods Mol. Biol.* **2007**, *392*, 183.
(9) Iqbal, A.; Wang, L.; Thompson, K. C.; Lilley, D. M. J.; Norman, D. G. *Biochemistry* **2008**, *47*, 7857.
(10) Mitra, R. D.; Silva, C. M.; Youvan, D. C. *Gene* **1996**, *173*, 13.
(11) Heim, R.; Tsien, R. Y. *Curr. Biol.* **1996**, *6*, 178.
(12) Okamura, Y.; Watanabe, Y. *Methods Mol. Biol.* **2006**, *335*, 43.
(13) Yea, K.-H.; Lee, S.; Choo, J.; Oh, C.-H.; Lee, S. *Chem. Commun.* **2006**, 1509.
(14) Ho, H. A.; Dore, K.; Boissinot, M.; Bergeron, M. G.; Tanguay, R. M.; Boudreau, D.; Leclerc, M. *J. Am. Chem. Soc.* **2005**, *127*, 12673.
(15) Tyagi, S.; Kramer, F. R. *Nat. Biotechnol.* **1996**, *14*, 303.
(16) Lakowicz, J. R.; Kusba, J.; Shen, Y.; Malicka, J.; D'Auria, S.; Gryczynski, Z.; Gryczynski, I. *J. Fluoresc.* **2003**, *13*, 69.
(17) Lakowicz, J. R.; Malicka, J.; D'Auria, S.; Gryczynski, I. *Anal. Biochem.* **2003**, *320*, 13.
(18) Lukomska, J.; Malicka, J.; Gryczynski, I.; Lakowicz, J. R. *J. Fluoresc.* **2004**, *14*, 417.
(19) Wokaun, A.; Lutz, H. P.; King, A. P.; Wild, U. P.; Ernst, R. R. *J. Chem. Phys.* **1983**, *79*, 509.
(20) Malicka, J.; Gryczynski, I.; Kusba, J.; Lakowicz, J. R. *Biopolymers* **2003**, *70*, 595.
(21) Malicka, J.; Gryczynski, I.; Fang, J.; Kusba, J.; Lakowicz, J. R. *Anal. Biochem.* **2003**, *315*, 160.
(22) Zhang, J.; Fu, Y.; Chowdhury, M. H.; Lakowicz, J. R. *J. Phys. Chem. C* **2007**, *111*, 11784.
(23) Zhang, J.; Fu, Y.; Lakowicz, J. R. *J. Phys. Chem. C* **2007**, *111*, 50.
(24) Aslan, K.; Wu, M.; Lakowicz, J. R.; Geddes, C. D. *J. Am. Chem. Soc.* **2007**, *129*, 1524.
(25) Viger, M. L.; Live, L. S.; Therrien, O. D.; Boudreau, D. *Plasmonics* **2008**, *3*, 33.
(26) Tovmachenko, O. G.; Graf, C.; van den Heuvel, D. J.; van Blaaderen, A.; Gerritsen, H. C. *Adv. Mater.* **2006**, *18*, 91.
(27) Cheng, D.; Xu, Q.-H. *Chem. Commun.* **2007**, 248.
(28) Stranik, O.; Nooney, R.; McDonagh, C.; MacCraith, B. D. *Proc. SPIE-Int. Soc. Opt. Eng.* **2005**, *5824*, 79.
(29) Zhang, J.; Fu, Y.; Chowdhury, M. H.; Lakowicz, J. R. *J. Phys. Chem. C* **2008**, *112*, 18.
(30) Liu, S.; Han, M. *Adv. Funct. Mater.* **2005**, *15*, 961.
(31) Liu, S.; Zhang, Z.; Han, M. *Anal. Chem.* **2005**, *77*, 2595.
(32) Imhof, A.; Megens, M.; Engelberts, J. J.; De Lang, D. T. N.; Sprik, R.; Vos, W. L. *J. Phys. Chem. B* **1999**, *103*, 1408.
(33) Aslan, K.; Leonenko, Z.; Lakowicz Joseph, R.; Geddes Chris, D. *J. Fluoresc.* **2005**, *15*, 643.
(34) Lakowicz, J. R.; Malicka, J.; Gryczynski, I.; Gryczynski, Z.; Geddes, C. D. *J. Phys. D: Appl. Phys.* **2003**, *36*, R240.
(35) Lakowicz, J. R. *Anal. Biochem.* **2001**, *298*, 1.
(36) Zhang, J.; Fu, Y.; Chowdhury, M. H.; Lakowicz, J. R. *Nano Lett.* **2007**, *7*, 2101.
(37) Zhang, J.; Fu, Y.; Chowdhury, M. H.; Lakowicz, J. R. *J. Phys. Chem. C* **2007**, *111*, 11784.
(38) Du, H.; Fuh, R.-C. A.; Li, J.; Corkan, L. A.; Lindsey, J. S. *Photochem. Photobiol.* **1998**, *68*, 141.
(39) Epe, B.; Steinhaeuser, K. G.; Woolley, P. *Proc. Natl. Acad. Sci. U. S. A.* **1983**, *80*, 2579.

NL901553U